11th International Workshop on Ship and Marine Hydrodynamics
Hamburg, Germany, September 22-25, 2019

Planar Motion Modeling of Full-Scale SUBOFF in Deep and Unlimited Water

Yu-Cheng Hsu, Chi-Yu Chen, Sheng-Hsuan Chiu, Shiu-Wu Chau*

National Taiwan University, Department of Engineering Science and Ocean Engineering
1, Sec. 4, Roosevelt Road, Taipei 10617, Taiwan

*Corresponding author, chausw@ntu.edu.tw

ABSTRACT

This paper proposes a numerical approach to predict the planar motion of a full-scale SUBOFF as well as its hydrodynamic coefficients in deep and unlimited water, where the free surface and wall effects are neglected. The Euler's equations of motions are employed to describe the underwater motion of a body in deep submergence. Due to the geometrical features of the studied hull form, a simplified form of motion equations is obtained through ignoring minor equation terms in the case of planar motions. A linear approach is further adopted to estimate the added mass and damping coefficients of the submerged vessel, where the coefficients of main components of vessel, such as hull, sail, sail fin, stern fin, and rudder, are separately evaluated and then integrated into the simplified motion equations. The turbulent flow around these components are numerically calculated to predict their hydrodynamic coefficients, where a grid-independent solution is predicted via a successive grid refinement of the computational domain. The solution of the simplified motion equations is based on a time-marching scheme. An iterative method is first used to solve the simplified motion equations at a given instance and a first-order projection method is then employed to predict the position and status of the vessel at the next time step.

1 INTRODUCTION

This paper investigates the planar motion characteristics of a Full-Scale SUBOFF (L=68 m) in deep and unlimited water [1,2], where the free surface and wall effects are completely ignored. The Euler's equations of motions are employed to describe the trajectory of an underwater body moving in deep submergence. The equations of motion equations are further simplified with the negligence of equation terms that are trivially contributed to a planar motion [3,4]. A linear approach is adopted to estimate the added mass and damping coefficients of a submerged body, where the coefficients of its main components, such as hull, sail, sail fin, stern fin, and rudder, Fig.1, are separately evaluated and then integrated into the adopted simplified motion equations. The hydrodynamic coefficients of these components are numerically estimated by means of a turbulent flow modeling, where the grid-independent solution is obtained through a grid refinement process. A time-marching scheme is adopted to solve the coupled simplified motion equations, where the time-dependent solution of the simplified motion equations is iteratively solved along with the position and status of the vessel calculated by a first-order projection method.

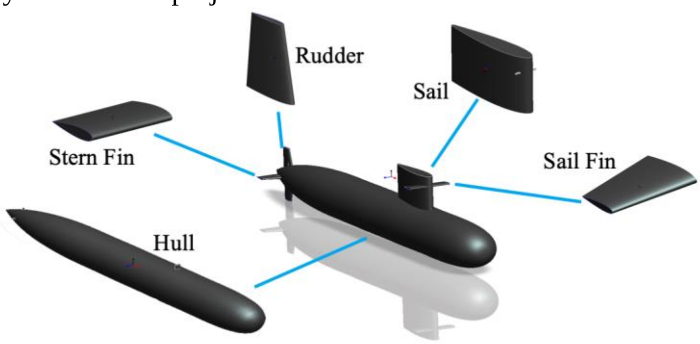

Figure 1: Main components of a submerged vessel

2 HYDRODYNAMIC COEFFICIENTS

2.1 Governing Equations

The incompressible continuity and momentum equations incorporated with an SST $k-\omega$ turbulence model are adopted to describe the turbulent flow around the submerged body:

$$\frac{\partial u_i}{\partial x_i}=0 \tag{1}$$

$$\frac{\partial u_i}{\partial t}+\frac{\partial(u_i u_j)}{\partial x_j}=-\frac{1}{\rho}\frac{\partial p}{\partial x_i}+\frac{\partial}{\partial x_j}\left[\nu\left(\frac{\partial u_i}{\partial x_j}+\frac{\partial u_j}{\partial x_i}\right)\right]+\frac{\partial}{\partial x_j}\left(\overline{u_i' u_j'}\right) \tag{2}$$

$$\frac{\partial k}{\partial t}+\frac{\partial(k u_j)}{\partial x_j}=-\overline{u_i' u_j'}\frac{\partial u_i}{\partial x_j}-\beta^*\omega k+\frac{\partial}{\partial x_j}\left[(\nu+\sigma_k\nu_t)\frac{\partial k}{\partial x_j}\right] \tag{3}$$

$$\frac{\partial \omega}{\partial t}+\frac{\partial(\omega u_j)}{\partial x_j}=\frac{\gamma}{\nu_t}\overline{u_i' u_j'}\frac{\partial u_i}{\partial x_j}-\beta\omega^2+\frac{\partial}{\partial x_j}\left[(\nu+\sigma_\omega\nu_t)\frac{\partial \omega}{\partial x_j}\right]+2(1-\delta)\sigma_{\omega 2}\frac{1}{\omega}\frac{\partial k}{\partial x_j}\frac{\partial \omega}{\partial x_j} \tag{4}$$

where u_i denotes the velocity component in the x_i direction, p the pressure, ν the kinematic viscosity, $\overline{u_i' u_j'}$ the Reynolds stress, t the time, k the turbulent kinetic energy, the dissipation rate of k, ν_i the turbulent kinematic viscosity and $(\sigma_k,\sigma_\omega,\sigma_{\omega 2},\beta^*,\beta,\delta)$ the turbulence model constants [5,6]. Equation (1) to (4) are numerically solved with the flow solver STARCCM+ to obtain the turbulent around the submerged body for the purpose to evaluate its hydrodynamic forces under various conditions.

2.2 Resistance Prediction

Figure 1 compares the measured and predicted model-scale resistance as well as the full-scale resistance components between numerical results and ITTC line. Figure 2(a) shows a good agreement of numerical prediction with experimental measurements for a bare hull SUBOFF model, whereas Figure 2(b) depicts the resistance comparison for a SUBOFF model with full appendages. Similar to the bare hull, the full-ship delivers a high resistance prediction accuracy. Figure 2(c) predicts the total resistance coefficient (C_T) varying between 2.2×10^{-3} and 2.6×10^{-3} for the five calculated velocities. The friction coefficient (C_F) following a similar tendency of ITTC line is estimated between 2.0×10^{-3} and 1.6×10^{-3}. The definition of the resistance coefficients and ITTC line are given in Eq. (5), (6) and (7), where R is the total resistance, ρ the density, u the ship speed, S the wetted surface, R_f the frictional drag. Figure 2 indicated the numerical prediction is able to deliver accurate hydrodynamic force exerted on a moving vessel.

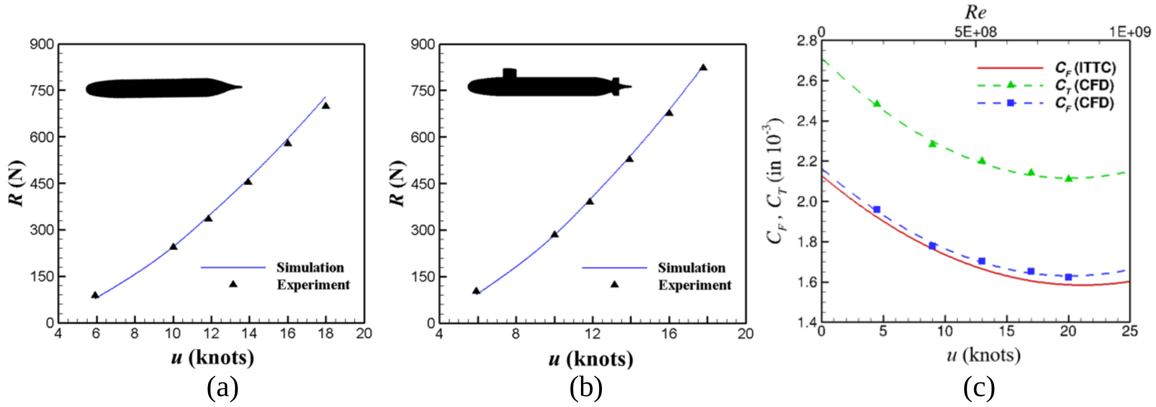

Figure 2: Resistance prediction – (a) Model scale (Bare hull), (b) Model scale (Full ship), (c) Full scale.

$$C_{T,CFD}=\frac{R}{\frac{1}{2}\rho u^2 S} \tag{5}$$

$$C_{F,CFD} = \frac{R_f}{\frac{1}{2}\rho u^2 S} \tag{6}$$

$$C_{F,ITTC} = \frac{0.075}{(\log(Re)-2)^2} \tag{7}$$

2.3 Added Mass

Because the bare hull is a slender body, only m_{11}, m_{22} and m_{33} are considered for the bare hull. The prediction of added mass is determined via the following procedure. The submerged body is modelled in the given linear motion with a constant acceleration (a) for a period of time. Then, the resistance experienced at different time instances is fitted with a polynomial function. The constant term of this polynomial function (f_0) represents the force acting on the vessel at *t*=0 in an acceleration motion from rest. The added mass (m_a) of a volume V corresponding to this motion is given as

$$m_a = \frac{f_0 - V \cdot a}{a} \tag{8}$$

An ellipsoid with an axis ratio of 2 is adopted to validate the proposed approach to calculate the added mass of a submerged body, where m_{22} is selected as the validation target. Figure 3(a) gives the history of dimensionless force (*Y'*) in an acceleration motion of 1.0 m/s^2 for various grid numbers, where *Y'* is fitted through a second-order polynomial. The grid-independent *Y'* at *t*=3 s (dotted line in red, 0.705) along with its counterparts with different grid density is illustrated in Figure 3(b), where the grid-independent history of *Y'* is given in Figure 3(c). The constant term of the fitted equation obtained from numerical prediction is 0.7043, which delivers an error less than 0.5% when compared to its theoretical value of 0.7020. Table 1 summarises the added mass of bare hull for a full-scale SUBOFF.

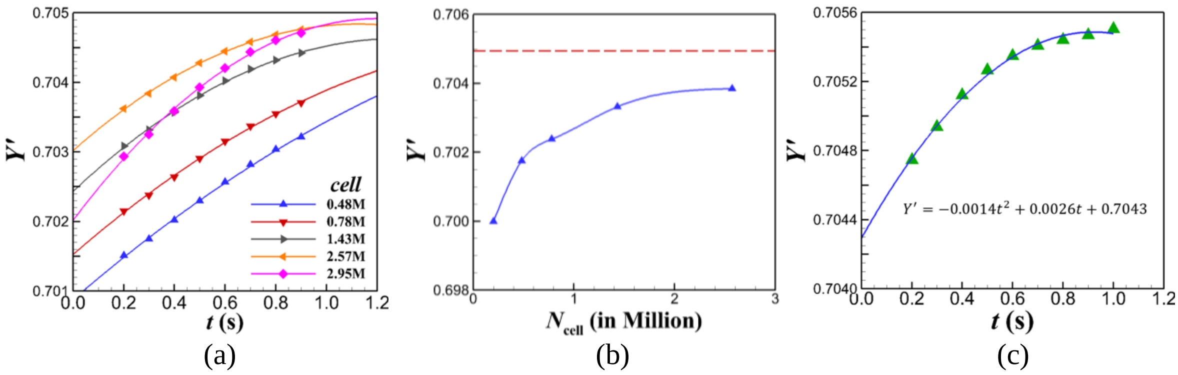

Figure 3: Added mass validation – (a) *Y'* with different grids, (b) *Y'* at *t*=3 s, (c) Grid-independent *Y'*.

Table 1: Added masses of SUBOFF bare hull on full scale

m_{11} (10^6kg)	m_{22} (10^6kg)	m_{33} (10^6kg)
0.103	2.43	2.43

2.4 Added Moment of Inertia

The added moment of inertia m_{44}, m_{55} and m_{66} are simply taken account for the bare hull due to its axisymmetric shape. The prediction of added moment of inertia is determined via the following procedure. The submerged body is modelled in the given rotational motion with a constant angular acceleration (ω) for a period of time. Then, the moment experienced at different time instances is fitted with a polynomial function. The constant term of this polynomial function (m_0) represents the moment acting on the vessel at *t*=0 in an angular acceleration motion from rest as well as the added moment of inertia. Table 2 summarises the added moment of inertia of SUBOFF bare hull on full scale.

Table 2: Added moment of inertia of SUBOFF bare hull on full scale

m_{44}(10^9kg·m^2)	m_{55}(10^9kg·m^2)	m_{66}(10^9kg·m^2)
~0	0.576	0.576

2.5 Viscous Drag

Due to a slim shape of bar hull and comparably small viscous drag in the lateral direction, only the longitudinal viscous drag is considered for the bare hull. The prediction of viscous drag is determined via the following procedure. The submerged body is modelled in the given linear motion with a constant velocity. Then, the resistance experienced at different velocities is fitted with a polynomial function that is employed in the motion simulation of the submerged body. Equation 9 gives a second-order polynomial to describe the bare hull drag in the longitudinal direction, where F_x is the longitudinal drag, (A, B, C) the fitting constants. Table 3 summarises the drag equation constants for the bare hull on full scale.

$$F_x = Au^2 + Bu + C \tag{9}$$

Table 3: Equation constant of SUBOFF bare hull on full scale

A	B	C
1311.00	955.61	-202.08

2.6 Hydrodynamic Centre

The hydrodynamic force acting on a moving body can be divided into lift and drag components, where the pitching moment refers to the combined moment contributed by lift and drag. At the hydrodynamic centre, the pitching moment is basically independent of the angle of attack of the inflow. In contrast to the centre of pressure, the net moment contributed by lift and drag is zero. According to this assumption, the longitudinal location hydrodynamic centre (x_{HC}) is defined in Eq.(10), where is the longitudinal location of the centre of gravity, M_0 and M_1 the moment created by an angle of attach of 0° and 1°, respectively, L_0 and L_1 the lift created by an angle of attach of 0° and 1°, respectively.

$$x_{HC} = x_G + \frac{M_1 - M_0}{L_1 - L_0} \tag{10}$$

3 EQUATION OF MOTION

The Euler's equations of motions based on a body-fixed frame is employed to describe the correlation among the velocity, angular and external forces acting on the submerged body, i.e., Eq. (11), (12), (13), (14), (15) and (16), Fig.4:

$$m[\dot{u} - vr + qw - x_G(q^2 + r^2) + y_G(pq - \dot{r}) + z_G(pr + \dot{q})] = X_F \tag{11}$$

$$m[\dot{v} - wp + ur - y_G(p^2 + r^2) + x_G(pq + \dot{r}) + z_G(qr - \dot{p})] = Y_F \tag{12}$$

$$m[\dot{w} - uq + vp - z_G(p^2 + q^2) + x_G(rp - \dot{q}) + y_G(rq + \dot{p})] = Z_F \tag{13}$$

$$\begin{gathered} I_{xx}\dot{p} + (I_{zz} - I_{yy})qr - I_{xz}(\dot{r} + pq) + I_{xy}(pr - \dot{q}) + I_{yz}(r^2 - q^2) \\ + my_G(\dot{w} + vp - uq) - mz_G(\dot{v} + ur - wp) = K_F \end{gathered} \tag{14}$$

$$\begin{gathered} I_{yy}\dot{q} - (I_{zz} - I_{xx})pr - I_{yz}(\dot{r} - pq) - I_{xy}(\dot{p} + qr) + I_{xz}(p^2 - r^2) \\ - mx_G(\dot{w} + vp - uq) + mz_G(\dot{u} - vr + wq) = M_F \end{gathered} \tag{15}$$

$$\begin{gathered} I_{zz}\dot{r} + (I_{yy} - I_{xx})pq - I_{xz}(\dot{p} - qr) - I_{yz}(\dot{q} + pr) - I_{xy}(p^2 - q^2) \\ + mx_G(\dot{v} + ur - wp) - my_G(\dot{u} - vr + wq) = N_F \end{gathered} \tag{16}$$

where m denotes the mass of the body, (u, v, w) the velocity of the body, (p, q, r) the angular velocity of the body, (x_G, y_G, z_G) the gravity centre of the body, $(I_{xx}, I_{yy}, I_{zz}, I_{xy}, I_{yz}, I_{xz})$ the moment of inertia of the body, (X_F, Y_F, Z_F) the external force acting on the body and (K_F, M_F, N_F) the external moment acting on the body. Equation (1) to (6) is numerically solved with the help of a first-order projection method to predict the position and status of the submerged body. A time-marching scheme is adopted to solve the coupled simplified motion equations, where the time-dependent solution of the simplified motion equations is iteratively solved along with the position and status of the vessel calculated by a first-order projection method. [1,2]

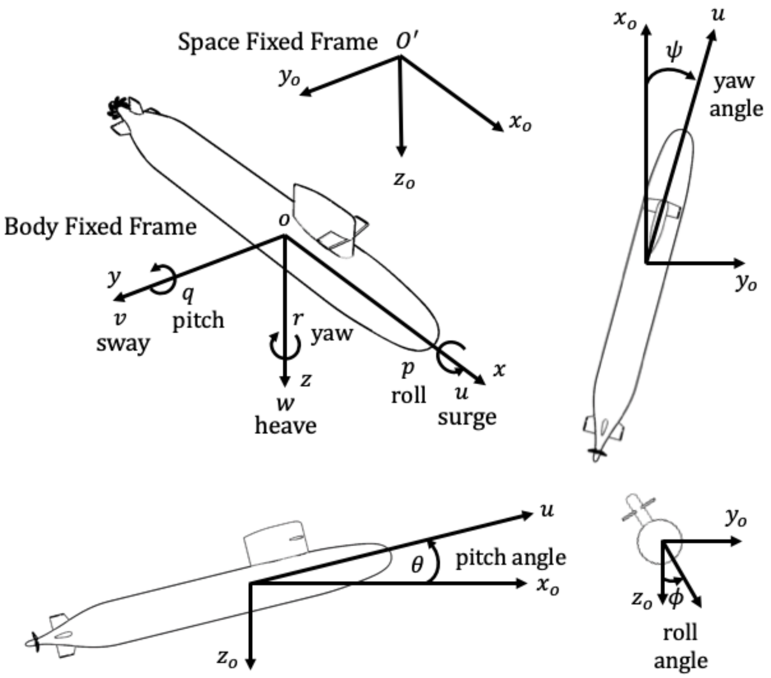

Figure 4: Definition of a six degree-of-freedom motion

4 MANOEUVRING SIMULATIONS

The propulsion characteristics identical to an affine hull form (L=66.9 m) [2] is adopted in this study to investigate the full-scale SUBOFF performance in a turning circle test as well as in a zigzag test. Figure 5(a) depicts the full-scale trajectory comparison between the studied SUBBOFF and an affine hull given in [2]. The turning circle test is simulated under a rudder angle of 15° and a propeller speed of 40 RPM. Table 4 summarises the key parameters of the turning circle test between SUBOFF and an affine vessel, where the former obtains a higher service speed with a smaller turning radius. Figure 5(b) shows the simulation of a zigzag test with a rudder angle of 20° that is identical to the executive heading angle, where the red line denotes the rudder angle and the green line the heading angle. The overshoot is predicted about 10 sec for SUBOFF, whereas the affine vessel is approximate 7.4 sec. Table 5 summarises the simulated result of a Zigzag test.

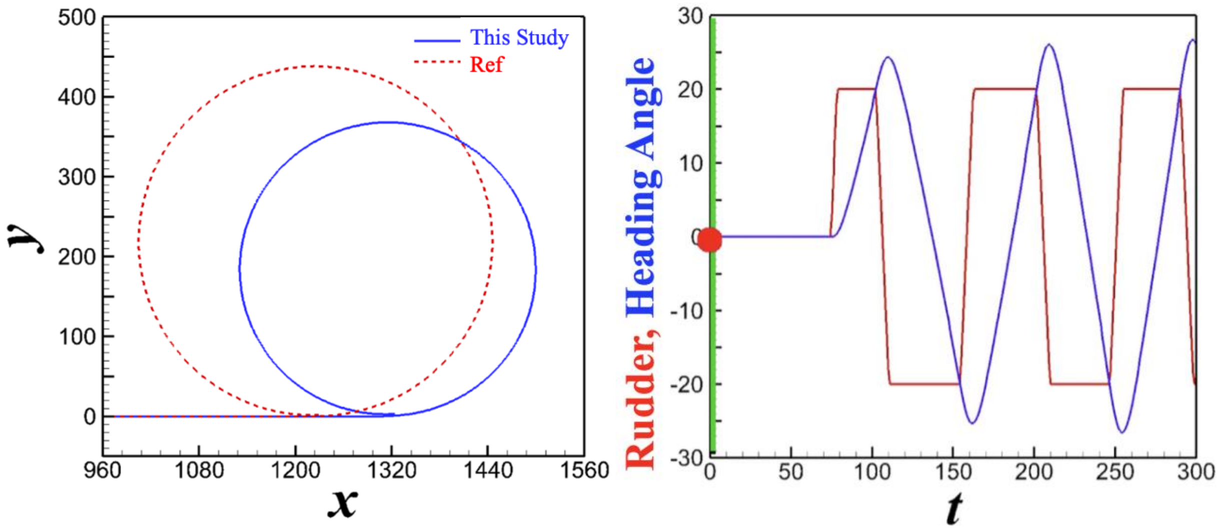

(a) (b)

Figure 5: Manoeuvring simulations – (a) Turning circle test, (b) Zigzag test.

Table 4: The comparison of turning circle test between two hull forms.

Hull Form	Speed (kn)	Advance (m)	Transfer (m)	Turning Radius (m)	Tactical Radius (m)
Affine	3.6	258	217	429	431
SUBOFF	3.9	231	183	365	368

Table 4: The comparison of turning circle test between two hull forms.

Hull Form	Initial Turning Time (s)	Overshoot (°)	Time to check yaw (s)	Reach (s)	Time of a complete cycle (s)
SUBOFF	100	10	10	135	195

5 CONCLUSION

This paper proposes a numerical approach to model the motion of a submerged vessel along with its hydrodynamic coefficients in deep and unlimited water, where the planar motion of a full-scale SUBOFF is predicted as an example. The resistance comparisons on model and full scale indicate that the adopted flow solver is capable of delivering accurate hydrodynamic loads around a submerged vessel as well as reliable hydrodynamic coefficients. This study suggest that the predicted turning diameter is 365 m along with a speed of 3.9 kn for a turning circle test of SUBOFF under a rudder angle of 15° and a propeller speed of 40 RPM, which is consistent with the performance of an affine vessel under the same condition. In the zigzag simulation, the full-scale SUBOFF gives an overshoot similar to its time to check yaw, 10 s, where its initial turning time, reach and time of a complete circle are 100s, 135s and 195s, respectively.

ACKNOWLEDGEMENTS

This paper is financially supported by the Ministry of Science and Technology, ROC under the Project No. MOST 106-2218-E-002-035.

REFERENCES

[1] Chang, Y.H. On a *Mathematical Model for Submarine Maneuvering Mmtion and Simulation.* Master Thesis, Dept. of Eng. Sci. and Ocean Eng., National Taiwan University, 2006.

[2] Liu, W.C. *Development for a Simulation System of Submarine Maneuvering Motions by Applying Modular Mathematical Model*. Master Thesis, Dept. of Eng. Sci. and Ocean Eng., National Taiwan University, 2015.

[3] Groves, N.C., Huang, T.T., and Chang, M.S. *Geometric characteristics of DARPA SUBOFF models: (DTRC Model Nos. 5470 and 5471)*. David Taylor Research Center, 1989.

[4] Roddy, R.F., *Investigation of the stability and control characteristics of several configurations of the DARPA SUBOFF model (DTRC Model 5470) from captive-model experiments*. David Taylor Research Center, 1990.

[5] Menter, F. *Zonal two equation k-w turbulence models for aerodynamic flows*. Proceedings of the 23rd fluid dynamics, plasmadynamics, and lasers conference, 1993.

[6] User Guide version 9.04. CD-adapco Corporation.